Dynamic regulation of spine–dendrite coupling in cultured hippocampal neurons

Eduard Korkotian,[1] David Holcman[2,3] and Menahem Segal[1]

[1]Department of Neurobiology and
[2]Department of Mathematics, The Weizmann Institute, Rehovot 76100, Israel
[3]Keck Center for Integrative Neuroscience, 513 Parnassus Ave, 94143–0444, San Francisco, California, USA

Abstract

We investigated the role of dendritic spine morphology in spine–dendrite calcium communication using novel experimental and theoretical approaches. A transient rise in $[Ca^{2+}]_i$ was produced in individual spine heads of Fluo-4-loaded cultured hippocampal neurons by flash photolysis of caged calcium. Following flash photolysis in the spine head, a delayed $[Ca^{2+}]_i$ transient was detected in the parent dendrites of only short, but not long, spines. Delayed elevated fluorescence in the dendrite of the short spines was also seen with a membrane-bound fluorophore and fluorescence recovery from bleaching of a calcium-bound fluorophore had a much slower kinetics, indicating that the dendritic fluorescence change reflects a genuine diffusion of free $[Ca^{2+}]_i$ from the spine head to the parent dendrite. Calcium diffusion between spine head and the parent dendrite was regulated by calcium stores as well as by a Na–Ca exchanger. Spine length varied with the recent history of the $[Ca^{2+}]_i$ variations in the spine, such that small numbers of calcium transients resulted in elongation of spines whereas large numbers of calcium transients caused shrinkage of the spines. Consequently, spine elongation resulted in a complete isolation of the spine from the dendrite, while shrinkage caused an enhanced coupling with the parent dendrite. These studies highlight a dynamically regulated coupling between a dendritic spine head and its parent dendrite.

Introduction

High resolution imaging of calcium variations in individual dendritic spines of living neurons has demonstrated that the spine is a unique calcium compartment (Guthrie *et al.*, 1991; Harris & Kater, 1994; Shepherd, 1996; Segal *et al.*, 2000; Nimchinsky *et al.*, 2002). Synaptic and chemical stimulation were used to raise $[Ca^{2+}]_i$ to higher levels in the spine head than in its parent dendrite (Yuste & Denk, 1995; Svoboda *et al.*, 1996; Sabatini *et al.*, 2002), supporting the assertion that the spine is independent of the parent dendrite. However, when calcium is released from stores, short spines were more coupled to their parent dendrites than long ones in the sense that the stores of the long spines tended to deplete faster than those of the short spines (Korkotian & Segal, 1998). Using fluorescence recovery from photobleaching or uncaging of fluorescein (Svoboda *et al.*, 1996), it has been calculated that equilibrium time constants between spines and dendrites are in the range 20–100 ms, suggesting that the path connecting the spine head with the parent dendrite is of relatively low resistance (4–50 MΩ), which is lower than previous estimates. However, the use of fluorescein for estimation of the dimensions of the diffusion space does not produce a realistic picture of spine–dendrite relations with respect to calcium ions, as calcium ions could be expected to behave in a narrow spine neck environment very differently from fluorescein. Likewise, activation of voltage-gated calcium channels in both the dendrite and the spine head by back-propagating action potentials (Segal, 1995; Majewska *et al.*, 2000a,b) makes it difficult to assess the diffusion of free calcium ions between the two compartments. Specifically, if $[Ca^{2+}]_i$ rises in the spine compartment within 2–5 ms after the transient rise in the parent dendrite, would it be safe to assume that this rise is caused by activation of voltage-gated channels on the spine head, or could it be caused by diffusion from the parent dendrite? Recently, flash photolysis of caged calcium has been used to produce local rises in free $[Ca^{2+}]_i$ (Brown *et al.*, 1999; Delaney & Zucker, 1990; Felmy *et al.*, 2003), allowing a direct test of spine–dendrite coupling with respect to calcium regulation. One other issue prompted the present study; if indeed spine length controls spine–dendrite coupling, and because spine length can change spontaneously and in response to stimulation, would the same spine change its coupling with the parent dendrite? Some preliminary studies indicate that it will (Majewska *et al.*, 2000b) but the current studies were designed to examine this issue in a more systematic manner. Both theoretical and experimental approaches can be used for addressing this question. We therefore set out to produce a frank comparison between flash-photolysed calcium and fluorescein in dendritic spines in cultured hippocampal neurons, as well as to develop a mathematical model in order to examine the extent of the neck barrier in the spine–dendrite coupling.

Materials and methods

Equipment

As an imaging platform we used an upright Pascal scanning confocal microscope (Zeiss) equipped with standard argon and HeNe lasers for excitation at wavelengths of 488 and 543 nm, respectively. An air-cooled tripled ND : YAG laser (New Wave Research Inc., Fremont, CA, USA; Korkotian *et al.*, 2004), emitting 355-nm, 3.6-mJ, 4.0-ns

single light pulses at a rate of 0.1–1 Hz, was used for the photolysis of caged molecules. The UV laser light was coupled to the confocal microscope using a dichroic mirror with high reflection at 355 nm and high transmission of visible light and was focused on the image plane through a 63×0.9 NA Achroplan water-immersion objective. A second laser, red helium–neon (1 mW, 632 nm; Melles Griot, Carlsbad, CA, USA), was used to align the UV laser in the field of view. The calculated UV light intensity amounted to 200–300 nJ, which produces a flux of $4–6 \times 10^{11}$ photons per pulse, focused on < 1 fL of medium containing from 1000 to 100 000 caged molecules. The acquisition program of line scans in the confocal microscope triggered the UV laser flash using a Master 8 stimulator (AMPI, Jerusalem, Israel).

Chemicals

Caged calcium (o-nitrophenyl EGTA-AM or the salt form), CMNB-caged fluorescein, X-Rhod-1 and Fluo-4AM were purchased from Molecular Probes, Inc., Eugene, OR, USA. Fluo-MOMO-AM was a gift from Teflabs Inc., Texas, USA. Thapsigargin was a gift from Alomone Laboratories, Jerusalem, Israel. All chemicals were aliquoted and frozen at −80 °C.

High resolution imaging of individual dendrites and spines

Hippocampal neurons were taken out of decapitated newborn rat pups, dissociated and plated on a glia bed on round glass coverslips, and grown *in vitro* for 2–4 weeks as detailed elsewhere (Goldin *et al.*, 2001). Cells were transfected with pDsRed (Clontech) 2–6 days before the experiment using lipofectamine 2000 (Pilpel & Segal, 2004). The coverglass was removed from the 24-well plate and was incubated for 1.5 h at room temperature with a mixture of 2 μM Fluo-4AM and 6 μM NP-EGTA-AM prepared in the recording medium. Alternatively, cells were injected in the recording stage under visual control with CMNB-caged fluorescein di-potassium salt (2 mM) or NP-EGTA tetra-potassium salt (6–10 mM), Alexa Fluor 555 (5 mM) and Fluo-4 (5 mM) using a sharp micropipette containing 1 M K-Acetate. Glasses were placed in the recording chamber, controlled by an automated X–Y stage (Luigs and Neumann, Ratingen, Germany) of the confocal microscope, where it was bathed in recording medium containing (in mM) NaCl, 129; KCl 4; $MgCl_2$ 1; $CaCl_2$ 2; glucose, 4.2; HEPES, 10; and TTX, 0.001. pH was adjusted to 7.4 with NaOH, and osmolarity to 320 mOsm with sucrose, at room temperature. In some experiments cells were recorded with a 1.5-mm OD patch pipette, containing (in mM) CsCl, 136; KCl, 10; NaCl, 5; HEPES, 10; EGTA, 0.1; MgATP, 1; NaGTP, 0.3; Phosphocreatine, 5; Alexa-Fluor 555, 0.1; and Fluo-4, 0.1. Osmolarity was 285 mOsm, pH 7.2. The signals were recorded with an Axopatch 200B amplifier (Axon Instruments, Union City, CA, USA). PClamp (Axon Instruments) and appropriate software (Synaptosoft Inc., Decatur, GA, USA) were used for data acquisition and analysis.

Images of 512×512 pixels were captured with the 63× water-immersion objective. Three-dimensional reconstruction of the dendrites was composed of successive 0.2–0.5-μm optical sections. A line was scanned through the centre of a spine–dendrite segment (0.7 ms per line) to detect fast changes in fluorescence following a flash of the UV laser. The imaging laser lights (488 and 543 nm) were reduced to 3–5% of nominal intensity. Using this setting, we were able to continuously stimulate the same spine–dendrite segment with no significant loss of reactivity due to dye bleaching or photodynamic damage. Also, baseline fluorescence was not reduced significantly, and transient fluorescence signals were reduced by up to 20% across the 1.5–2-h observation times, indicating that the cells were viable for the duration of the

experiments. Another indication of this fact involved the assessment of the morphology of the transfected neurons; healthy cells had smooth dendrites and these swelled up when the cell began to deteriorate. Data were not collected from such cells. The dendritic segments selected for the analysis in the present study had medium-sized spine heads (1.05 ± 0.12 μm) and varied in length from being stubby, < 0.5 μm, to long, > 2 μm. We avoided measuring calcium signals from headless spines or from uncharacteristically long ones (> 4 μm). Images of the spines were taken at high resolution several times during the experiment, using the red wavelength. Rest periods of 5–10 min were taken between sessions of UV pulses to allow cells to recover. Two-dimension images of Fluo-4 fluorescence were not taken because of low resting fluorescence levels. In some cases, the diffusion of calcium across the spine neck into the parent dendrite was estimated by dividing the spine neck into three continuous regions of interest and calcium changes were averaged in these regions. In all other cases, the spine neck was treated as a unique single compartment. Data were analysed using Matlab-based programs and *t*-tests or ANOVA, as appropriate. Curve fitting was done with KaleidaGraph software. The data were occasionally smoothed to reduce noise in the records, using standard smoothing functions. However, no smoothing was used to determine latency and peak responses, which were done automatically using Matlab software. Threshold was determined when the line passed 3 SD above the averaged initial levels of fluorescence. Background noise was subtracted in all linescan recordings before calculation of $\Delta F/F$.

Results

Mean time for calcium diffusion through the spine neck

Flash photolysis of caged calcium at the spine head produced a fast, 1–2-ms, rise and transient, 10–20-ms-long, decay of $[Ca^{2+}]_i$ in the spines, and a delayed rise of $[Ca^{2+}]_i$ in the spine neck and the parent dendrite. The delayed response in the parent dendrite resulted from diffusion of elevated calcium levels and not from direct photolysis of calcium in the parent dendrite; when the laser light was aimed at a spot which is ∼ 1 μm away from the spine head, no $[Ca^{2+}]_i$ rise was seen in either the spine or dendrite compartment (Fig. 1, A3, bottom). The responses to the flash photolysis were stable, and reproducible responses to the stimulation, applied at a rate of 1 Hz, could be recorded (Fig. 1B). The $[Ca^{2+}]_i$ rise initiated in the spine head was progressing at an initial rate of ∼ 1 μm/ms along the spine, but was delayed at the entry to the parent dendrite (Fig. 1, A3).The decay of elevated calcium was rather fast and could be described by a sum of two exponential rates, with time constants of ∼ 9 and 100 ms (see below).

Obviously, the use of Ca dye introduces an artifact which may affect calcium dynamics. This problem will be discussed below. Here, to estimate the time course of free calcium dynamics in a typical spine, we performed the following computations.

Computations

The mean time τ for calcium ions to arrive at the dendrite when the ions are initially located in the spine head can be decomposed into the sum of two mean times: first, the time τ_1 it takes for the ions to reach the entrance of the neck connected to the spine head and, second, the time τ_2 to travel through the neck to the dendrite. Because the surface of the spine neck is relatively small compared to the total surface of the spine head, the mean time τ_1 is equal to the time to find the entrance of the neck. This mean time has been computed in dimension 3 (Grigoriev *et al.*, 2002) as

$$\tau_1 = V/(4D\varepsilon) \quad (1)$$

where D is the diffusion constant, V is the volume of the spine head and ε is the radius of the spine neck.

In a one-dimensional approximation, the mean time τ_2 to travel through the neck and reach the dendrite (a reflective boundary condition is imposed at the connection between the spine head and the neck) is given by

$$\tau_2 = L/(2D) \quad (2)$$

where L is neck length. The total characteristic time τ is given by

$$\tau = \tau_1 + \tau_2 = V/(4D\varepsilon) + L/(2D) \quad (3)$$

For $V = 1 \ \mu m^3$, $D = 400 \ \mu m^2/s$, $\varepsilon = 0.1 \ \mu m$ and $L = 1 \ \mu m$, the mean time to find the neck entrance is $\tau_1 = 6.5$ ms while the time to travel through the neck is $\tau_2 = 1.25$ ms and the total time is

$$\tau = 6.5 + 1.25 = 7.75 \ \text{ms}. \quad (4)$$

These values represent the mean time for a system of particles to reach the spine neck and the dendrite. Naturally, the threshold latency will be faster than these values. Thus, in the absence of removal mechanisms, including buffers and pumps, the rate of diffusion into the parent dendrite is expected to be slower than the observation we made in the experiments.

Effect of spine length on calcium diffusion

We compared responses of shorter and longer spines, both at the spine head, and of the parent dendrites. While the initial response in the spine head was the same for either short or long spines (Fig. 2, B1) there was no significant difference in the decay time constants for the different spines, with the shorter spines having slightly shorter decay time constants ($\tau = 9.4$ and 99 ms for the long spines and 8.36 and 112 ms for the medium or short spines). However, there was a significant nonlinear relationship in the efficacy of the entry of calcium signal into the parent dendrite: the longer spines produced a much smaller and slower response in the parent dendrite than expected on the basis of the length of the spines (Fig. 2B–D). In fact, spines that were > 1.5 μm produced no change in $[Ca^{2+}]_i$ in the parent dendrite.

To examine the possibility that spine head diameter may contribute to the calcium responses we grouped the different spines into those with a large head (mean $1.36 \pm 0.07 \ \mu m$) and those with a small head ($0.78 \pm 0.05 \ \mu m$). There was no significant correlation between the parameters of the calcium transient and the size of the spine head, indicating that variations in the volume of the spine head by themselves did not contribute significantly to the dissipation of the excess calcium.

The observed change in fluorescence in the parent dendrite following uncaging of calcium in the spine head was assumed to result from diffusion of calcium ions from the spine head, but it could also reflect one of several other possible responses. In preliminary studies we verified that the diameter of the effective flash in our testing conditions is < 1 μm (Korkotian *et al.*, 2004) and so it is unlikely that we activated the parent dendrite directly in the short spines. This is also evident in the distinct delay of 2–3 ms in the dendritic responses relative to the spine responses. Second, it is possible that the flash activated calcium in presynaptic terminals (Felmy *et al.*, 2003) to cause release of glutamate and produce a synaptic response in the spine head. To rule this out, we conducted experiments in the presence of glutamate antagonists (20 μM DNQX and 50 μM 2-APV). Five medium and seven long spines were examined. Neither the latency and duration nor the amplitudes of the responses were different from the control cells studied in the absence of glutamate antagonists (data not shown), indicating that the transient calcium response seen in the spine head was probably not mediated by release of glutamate from presynaptic terminals.

Another possible source of the $[Ca^{2+}]_i$ rise is in other neuronal or glial elements in the field of view that are likely to take up the dye and the EGTA and produce a response that is not necessarily within the imaged pDsRed-transfected neuron. To rule this out, we injected nontransfected neurons with a mixture of Fluo-4 pentapotassium salt (5 mM), Alexa-Fluor 555 and NP-EGTA salt (6–10 mM) via a sharp micropipette that also contained 1 M K-acetate. The pipette was withdrawn after injection of the dye, and spines in these cells were subsequently imaged and analysed. In > 20 spines measured with this method, the results were similar to those produced in the standard method, indicating that the fluorescent signals were indeed originating in the imaged dendrites and spines and not in other neurons or glia (data not shown).

Effect of calcium dye on calcium diffusion

There is a possibility that spine-originated flash-photolysed calcium was indeed localized to the spine head but that, once bound to Fluo-4, it traveled through the spine head to the parent dendrite. Thus, it was not the free calcium diffusion that had been detected in the parent dendrite but the Fluo-4-bound one, which is of course an artifact of the measurement and not a genuine diffusion of calcium ion. The likelihood of this possibility was examined in our theoretical computations (below) and in the following experiments.

First, we estimated the dye concentration in the neurons under our testing conditions. This was done by clamping extracellular calcium at different concentrations, using the Molecular Probes kit, followed by the use of a calcium ionophore, and by blocking the involvement of calcium stores with thapsigargin (see below) to estimate fluorescence under different concentrations of dye and $[Ca^{2+}]_i$. This analysis resulted in an estimate of Fluo-4 dye inside the cell to be between 2 and 4 μM, which is slightly higher than the estimate provided by the catalogue of Molecular Probes Inc. for the same testing conditions but much below the concentration of dye used in similar experiments by others.

Second, we imaged calcium transients in cells loaded with a membrane-bound lipophilic analogue of Fluo-4 (Fluo-MOMO-AM; Teflabs Inc). In principle, this dye is bound to the membrane and cannot move from one cellular compartment to another following binding of free $[Ca^{2+}]_i$. Indeed, cells loaded with this dye had a very low background fluorescence in their nuclei and a marked staining of intracellular particles, yet they still produced spontaneous fluctuations of $[Ca^{2+}]_i$, in association with spontaneous spike discharges, as seen with Fluo-4 (data not shown). In 18 spines tested (Fig. 3), flash-photolysed calcium caused a transient elevation in Fluo-MOMO fluorescence, akin to that produced by Fluo-4. Interestingly, the decay of the elevated fluorescence signal was slower than that sampled by Fluo-4, probably due to slowed dissociation rate of Fluo-MOMO–calcium complex. Most importantly, the calcium signal was elevated in the parent dendrite just as it was in Fluo-4-loaded cells and, with about the same latency, for shorter spines. These experiments clearly indicate that calcium ions travel from the spine head through the neck
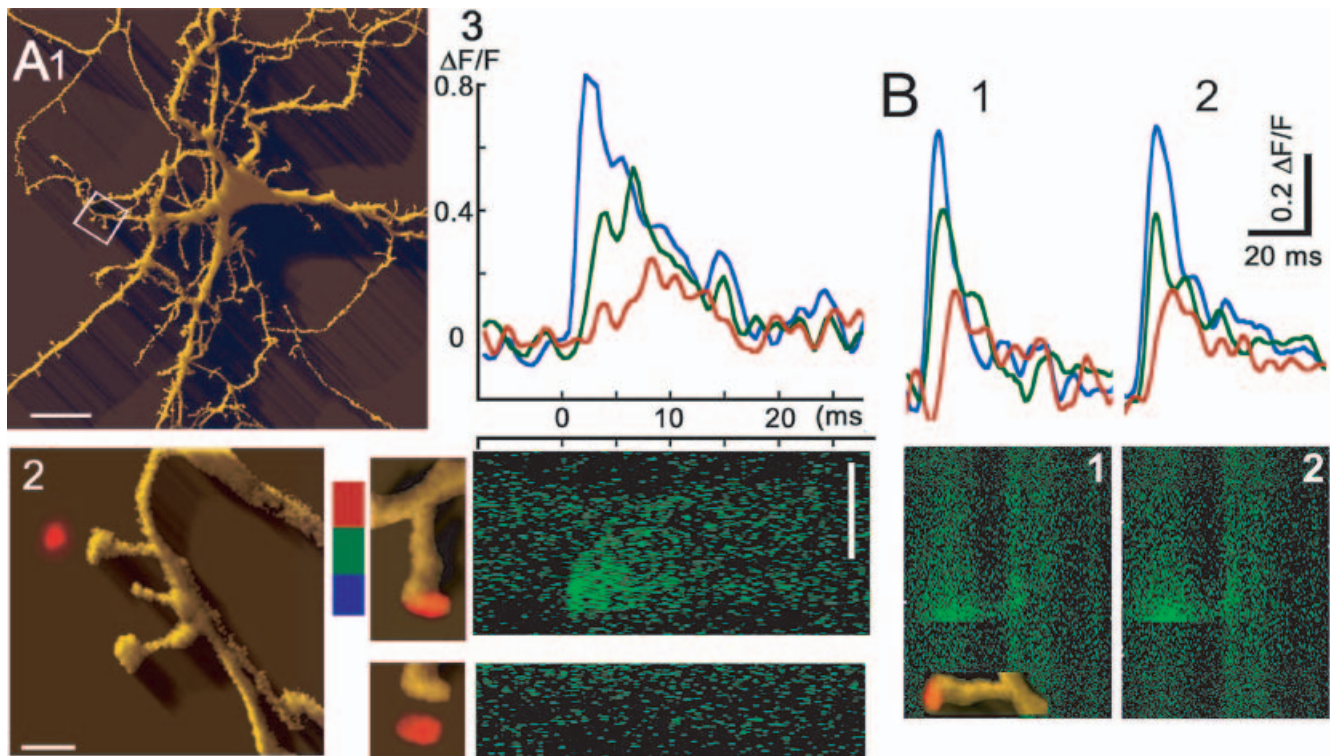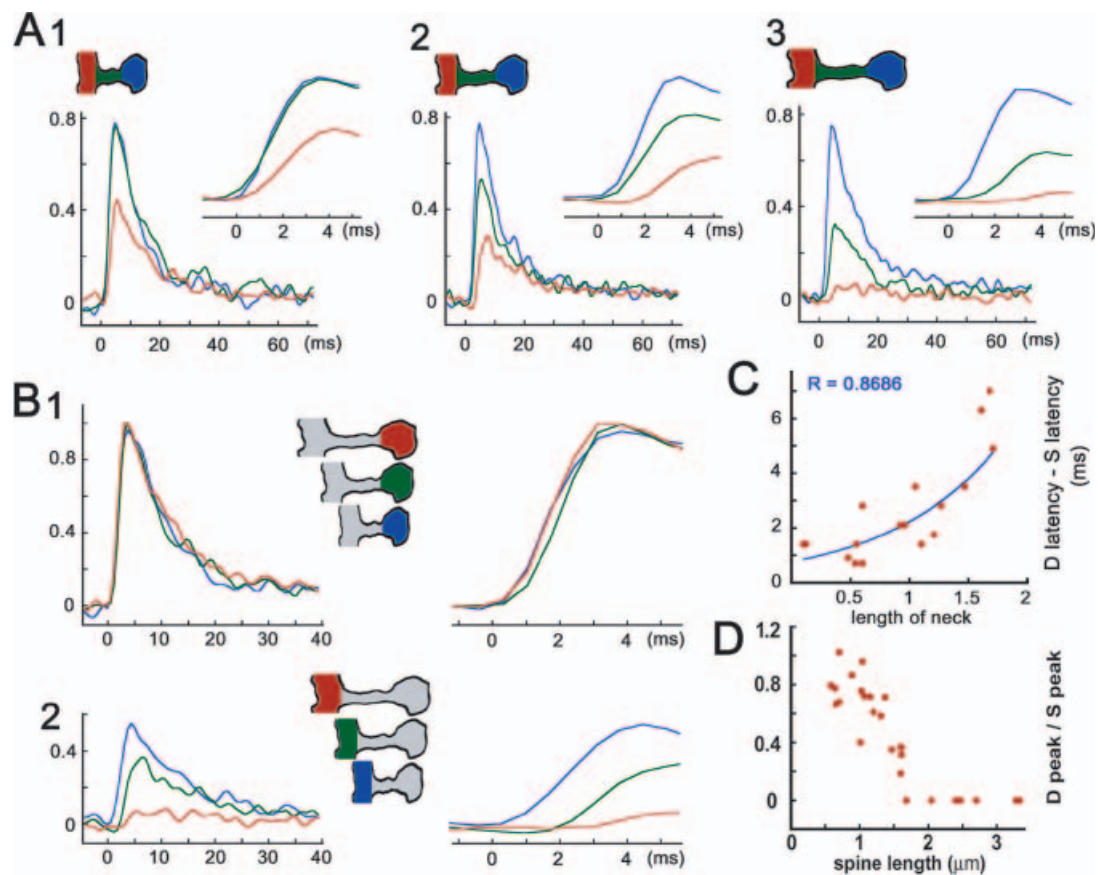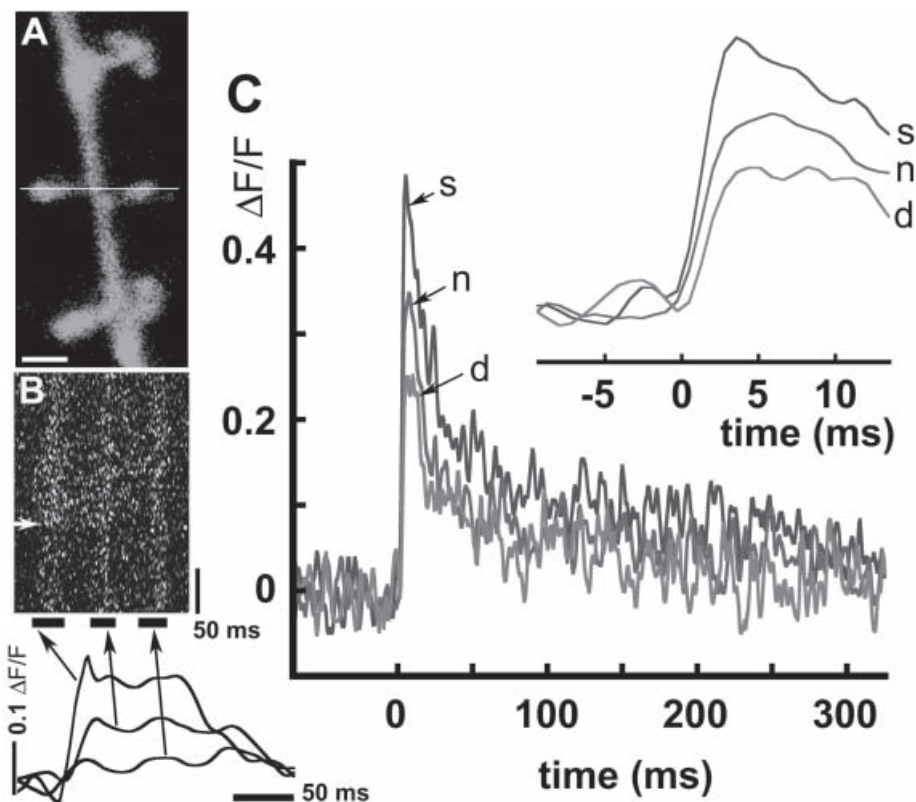
FIG. 1.

FIG. 2.

FIG. 3. Transient fluorescence changes upon uncaging of calcium, detected with a membrane-bound Fluo-MOMO dye. (A) A dendritic pDsRed-imaged segment, showing two spines, and a line scanned through them. (B) Line scan at the line shown above, from bottom to top; a flash was applied at the arrowhead causing a rise in fluorescence in the spine head and the parent dendrite. Note the colour bar, and the changes summarized below, of the same spine. A change is seen in the parent dendrite, middle, but not in the spine opposite to the exposed one (right). (C) A summary of responses of 18 spines to uncaging of calcium in the presence of Fluo-MOMO. A distinct response in the parent dendrites is seen, with a short delay (seen better in the average trace expanded in the insert). Note that the decay of the elevated fluorescence is much slower than that of Fluo-4. Scale bar, 1 μm (A).

to the parent dendrite in an unbound state, where they then bind to a local calcium-sensitive fluorescent dye.

Finally, we examined the mobility of a fluorescent calcium dye recovering from photobleaching at the spine head, and compared it to recovery from bleaching at the parent dendrite (Fig. 4). Before the

imaging experiments, cells were stably depolarized with high KCl-containing medium to enhance Fluo-4 fluorescence. Imaging experiments were conducted with the Zeiss 510 confocal microscope, which allows fast transitions between lines of the two wavelengths using acousto-optic modulation. Measurements were taken simultaneously

FIG. 1. Flash photolysis of caged calcium caused a transient local rise in $[Ca^{2+}]_i$. (A1) Image of a neuron that had been transfected with pDsRed for 2 days, and reconstructed in 3-D on the Pascal confocal microscope. The region marked with a rectangle is zoomed in A2. (A2) High power image of the dendrite marked in A1, with a red laser dot on the left to illustrate the size of the UV laser flash. (A3, bottom left) Two high magnification images of the spine are shown with the red laser dot on and near the spine head. The image is aligned with the line scan on the right, which runs from left to right, at the time scale indicated on top (in ms). Time resolution, 0.7 ms. A region of high fluorescence rising with the shortest latency at about the spine head is shown. Below, when the light spot is focused outside the spine head there is no evoked fluorescence in response to the light flash, applied at the same time as above. The colour code shown to the left of the spine represents the three compartments, the spine head (blue) neck (green) and the parent dendrite (red), which were analysed in A3, top. The curves show fluorescence changes in the spine compartments following flash photolysis of caged calcium in the spine head. A delay in response latencies between spine head and the parent dendrite is obvious. (B) Consistency of response across successive trials with the same spine, illustrating a peak response at the spine head (insert at image 1), and a smaller response at the neck (green) and the parent dendrite (red). Spine size 1 μm. Scale bars, 5 μm (A1), 1 μm (A2).

FIG. 2. Neck length determined spine head effects on dendritic $[Ca^{2+}]_i$. (A) Means of responses of groups of spines to evoked rise in $[Ca^{2+}]_i$ in spine head. (A1) In short spines ($n = 8$) the response in the parent dendrite amounted to ~60% of the response in the spine head. (A2 and A3) Medium sized and long spines ($n = 10$ and 15, respectively), where the responses in the parent dendrites were progressively smaller than the responses in the spine heads. Inserts demonstrate expanded traces of the rise time of the onset of responses. Colour codes are indicated in the inserts and represent spine, neck and dendrite compartments. (B) Comparisons of the responses of the different compartments in the three groups of spines. While the responses in the spine heads are the same (B1), the responses in the parent dendrites are remarkably different, depending on the spine neck length (B2). On the right are expanded time scales of the rise times of responses listed on the left. (C) The latencies of the responses in the parent dendrites are correlated with the spine neck length; the longer the neck, the slower the latency. A nonlinear fit ($r = 0.87$) describes the data better than a linear fit ($r = 0.79$). Note that only those cases are presented for which the dendrite transient latencies have been reliably calculated. (D) Calculated coupling index [(peak dendritic $\Delta F/F$)/(peak spine $\Delta F/F$)] indicates that the responses in the parent dendrites are correlated with spine neck length ($r = 0.89$), with the dendrites of the longer spines showing no change in calcium levels.
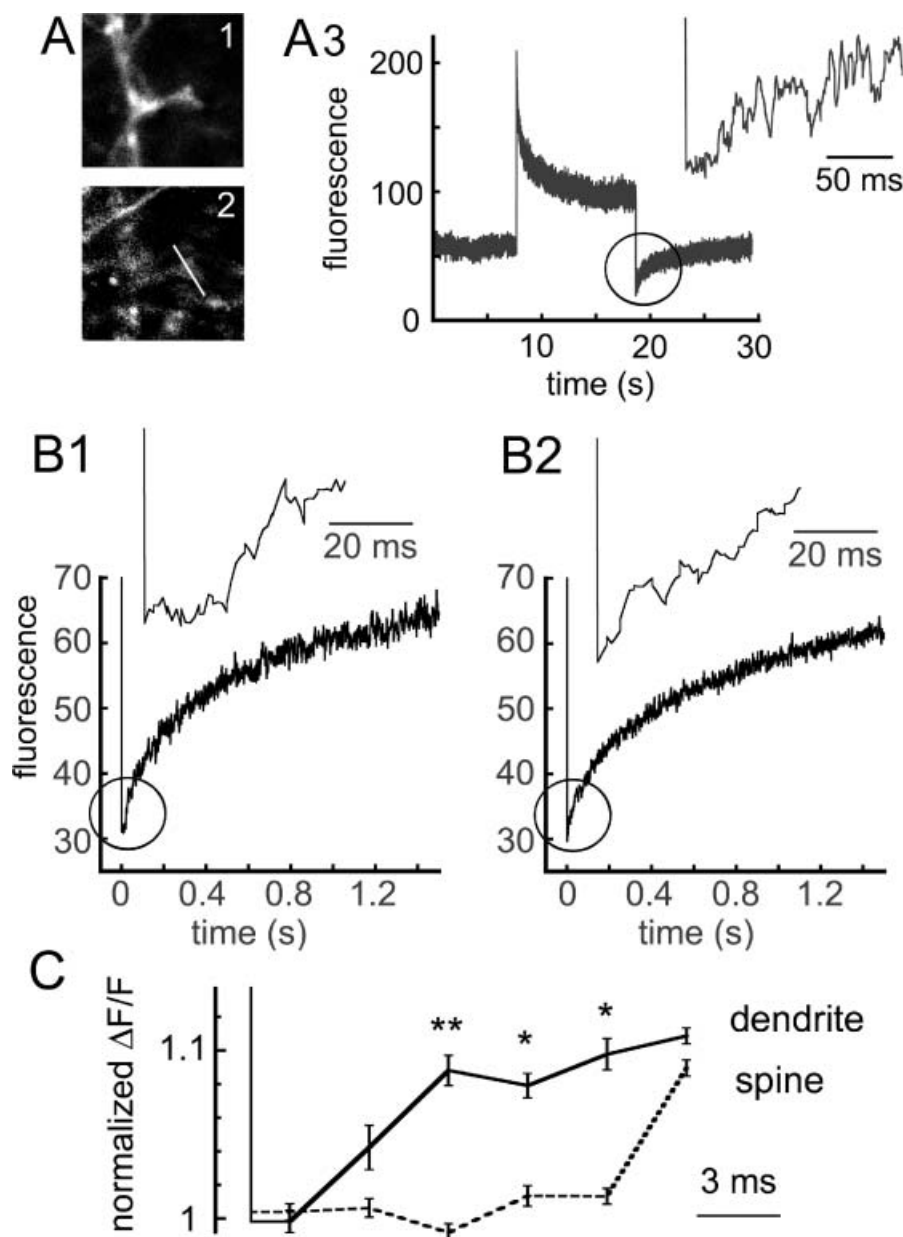
FIG. 4. Time course of recovery of fluorescence following bleaching in dendritic spine heads. (A) A pDsRed-transfected neuron was loaded with Fluo4 AM dye and imaged at 545 and 488 nm. A line was scanned through the spine head (A1 and 2). During the scan (A3), when the fluorescence level was stable, fluorescence intensity was raised to maximum in the 488-nm channel and a rapid decay of fluorescence was immediately seen. Upon return to the original imaging intensity a slow recovery of fluorescence was evident. An expanded trace (A3, insert) shows a distinct delay of ~ 20 ms before the beginning of the recovery. (B) Grouped data, comparing recovery following bleach at spine heads (B1), and at parent dendrites (B2), where no such delay was seen. (C) Statistical comparisons of the time course of fluorescence recovery following bleaching in dendrites and spines. Normalized fluorescence levels were averaged every 3 ms in the two samples and compared using *t*-tests; *$P < 0.05$, **$P < 0.001$. The recovery of fluorescence was significantly slower in the spine than the parent dendrites by at least 15 ms.

from the red channel and the green channel, which was bleached by high intensity light. Bleaching was conducted using line scan mode (~ 1 ms/line) by scanning the spine head or parent dendrite at high (100%) laser intensity for ~ 5 s followed by a rapid switch back to the standard illumination level (4% of nominal intensity).

The progress of an experiment is illustrated in Fig. 4, B1 and 2. The fluorescence level was high and decayed rapidly during the high intensity illumination which, however, did not affect the green fluorescence of the same spines. Following the switch to low level illumination, an apparent slow recovery of fluorescence at the spine head was evident. The overall kinetics of recovery of spine fluorescence (Fig. 4, B1) was similar to that of the recovery at the dendritic location (Fig. 4, B2). Surprisingly, there was a significant delay of ~ 20 ms before onset of recovery at the spine head compared to the recovery at the dendritic bleaching location ($n = 17$ dendrites, 19 spines; ANOVA, $P = 0.006$; Fig. 4B and C). This may account for the travel time along the spine neck between the parent dendrite and the spine head. If so, these results strongly suggest that the diffusion of a fluorescent dye is slower than that of a calcium ion, which reaches the parent dendrite with an initial latency of 2–3 ms.

To verify that the slow recovery from bleaching is not a function of the specific fluorophore, we repeated the experiments using GFP-transfected cells incubated for 1 h with X-rhod1AM dye, known to have relatively higher basal fluorescence. The results of these experiments were similar to those with the Fluo-4AM in pDsRed cells (data not shown; 16 spines and 11 dendritic segments).

Comparing calcium and fluorescein dynamics

We compared the kinetics of calcium transients with that of caged fluorescein, a neutral fluorescent molecule. While uncaging of fluorescein produced a fluorescence change with a similar latency and magnitude to that produced by calcium (Fig. 5), the decay time constant of the elevated fluorescence was markedly prolonged relative to that of calcium. As in the calcium decay kinetics, that of fluorescein could be fitted best by a sum of two exponentials, with the two time constants varying between short and long spines, the long ones having time constants of 33.8 and 240 ms and the short and middle ones having time constants of 26.2 and 245.8 ms ($n = 9$ and 10 spines, respectively). When measuring the half (50%)-decay times, which reflect the combined contributions of the two decay time constants, the results amounted to 86.5 ± 4.2 ms for the long spines and 65.8 ± 3.92 for the medium and short ones ($n = 9$ and 10 spines, respectively; $P < 0.02$). This is in sharp contrast to the half-decay of calcium, which amounted to 8.75 ± 0.35 ms for the long spines and 8.6 ± 0.7 ms for the medium and short spines.

Interestingly, the peak of the dendritic fluorescein transient in the short spines was slower than that of calcium (Fig. 5, B2). Having the same threshold of response, the slower peak indicates that fluorescein diffused more slowly than calcium towards the parent dendrite. This contrasts with an identical peak for the two fluorophores at the spine head (Fig. 5, B1). This also indicates that diffusion through a narrow neck can vary considerably depending on the dimensions of the diffusing molecule.

There was an obvious difference in the correlation coefficient relating length of the spines to the magnitude of the dendritic response, between the spines responding to fluorescein and those responding to a calcium surge (compare Figs 2D and 5C); while the dendrites did not show a calcium surge if the spines were > 1.5 μm they still responded to fluorescein, indicating that the spine neck is much more of a barrier for the transfer of calcium to the dendrite than for the transfer of fluorescein. This difference in the longer spines was highly significant (two-way ANOVA, $P < 0.01$) in both spine length and fluorophore, and in the interaction between the two parameters.

The time course of fluorescein dynamics, that is, the mean time it takes for this molecule to arrive at the dendrite when it appears inside the spine head, can be computed from equation (3) and is equal to 31 ms, in comparison to the 9 ms obtained above for calcium ions.

Calcium dynamics in spines following activation of voltage-gated calcium channels

The striking contrast between the decay time of elevated $[Ca^{2+}]_i$ in the present study (< 9 ms) and that reported elsewhere (> 50 ms; Majewska *et al.*, 2000a) can result from several factors, including the use of back-propagating action potentials as a means to raise $[Ca^{2+}]_i$ as well as a higher concentration of the indicator dye used in other studies. We patch-clamped neurons with Fluo-4 (100 μM) and Alexa Fluor 555 (100 μM) dyes, and recorded the fluorescence transients in spine–dendrite pairs while evoking calcium current by a 40-mV step depolarization of the soma from the holding potential of −55 mV (Fig. 6). Calcium transients were recorded from 33 such pairs in 19 neurons. The mean change in spine fluorescence was similar to that produced by the uncaging of calcium ($\Delta F/F = 1.76 \pm 0.14$), yet the dendritic response was significantly larger than the spine response ($\Delta F/F = 2.07 \pm 0.18$, $P < 0.001$), unlike the case with the uncaged calcium. In addition, some spines (e.g. Fig. 6A, left spine and Fig. 6F) responded with a smaller and slower rise in $[Ca^{2+}]_i$ than the dendritic responses. In fact, only about one third of the spines that were measured responded to the calcium surge in the spine with about the same latency (0–2 ms difference) as the parent dendrite, indicating that they may not express genuine voltage-gated calcium channels and that they only respond to changes taking place in the parent dendrite.

The decay kinetics of elevated $[Ca^{2+}]_i$ following activation of calcium currents was also markedly slower than the value obtained for the uncaged calcium, amounting to a median τ of 310 ms. This marked difference between the two cases of a calcium transient cannot be accounted for solely by the difference in dye concentration, as the concentration of the high buffer (40 μM, above) produced a slower decay, as expected, but not nearly as slow as this case. Other factors involved may have to do with the kinetics of the calcium channel or with the simultaneous increase in spine and dendritic shaft $[Ca^{2+}]_i$, preventing the diffusion of calcium from the spine head to the dendrite. At any rate, it is obvious that a rise in $[Ca^{2+}]_i$ evoked by release of caged calcium produces the fastest decay in spine calcium recorded to date.

Ongoing changes in spine–dendrite coupling

The functional relevance of the spine neck barrier was examined with spines that had changed their sizes during the recording session. Spines could elongate, shrink or express both elongation and shrinkage within 2 h of the observation time. In general, spines that had elongated lost their ability to produce calcium changes in the parent dendrites, whereas parent dendrites of spines that had shrunk began to respond to calcium transients originating in the spine head (Fig. 7B). The change in spine length was not usually associated with a change in spine head diameter (1.05 ± 0.12 μm in control, 1.08 ± 0.16 μm in shrunken spines, 1.12 ± 0.13 μm in elongated ones), but with a change in spine neck diameter such that shrunken spines had a slightly larger neck diameter than the elongated ones (0.37 ± 0.08 and 0.25 ± 0.07 μm, respectively), which caused a further increase in spine–dendrite coupling.

Strikingly, the direction of change in spine length was highly correlated with the number of calcium transients produced in the spine head; exposure to a low number of UV flashes (< 20, applied at a rate of 0.1 Hz) was associated with spine elongation whereas a larger number of calcium transients caused shrinkage of the spines by up to 0.5–1 μm (Fig. 7A–E). For all spines tested, during a control period of ∼ 10 min when spines were not exposed to repetitive pulses of calcium, no significant change in length or neck diameter was found (1.81 ± 0.12 and 0.25 ± 0.04, respectively, before, and 1.78 ± 0.11 and 0.27 ± 0.05, respectively, after; $n = 33$). Furthermore, no significant changes in spine length and no calcium transients were found in three spines exposed to UV flashes in the absence of NP-EGTA, indicating that calcium variations actually determine the dimensions of the spine, as suggested before (Korkotian & Segal, 1999). The latency of $[Ca^{2+}]_i$ transients recorded in different compartments was dependent on the dynamic changes of spine length (Fig. 7F and G), being about the same in the spine heads before and after the changes of spine dimensions while in the dendrites they appeared to be more than twice as large after spine elongations than after their shrinkage.
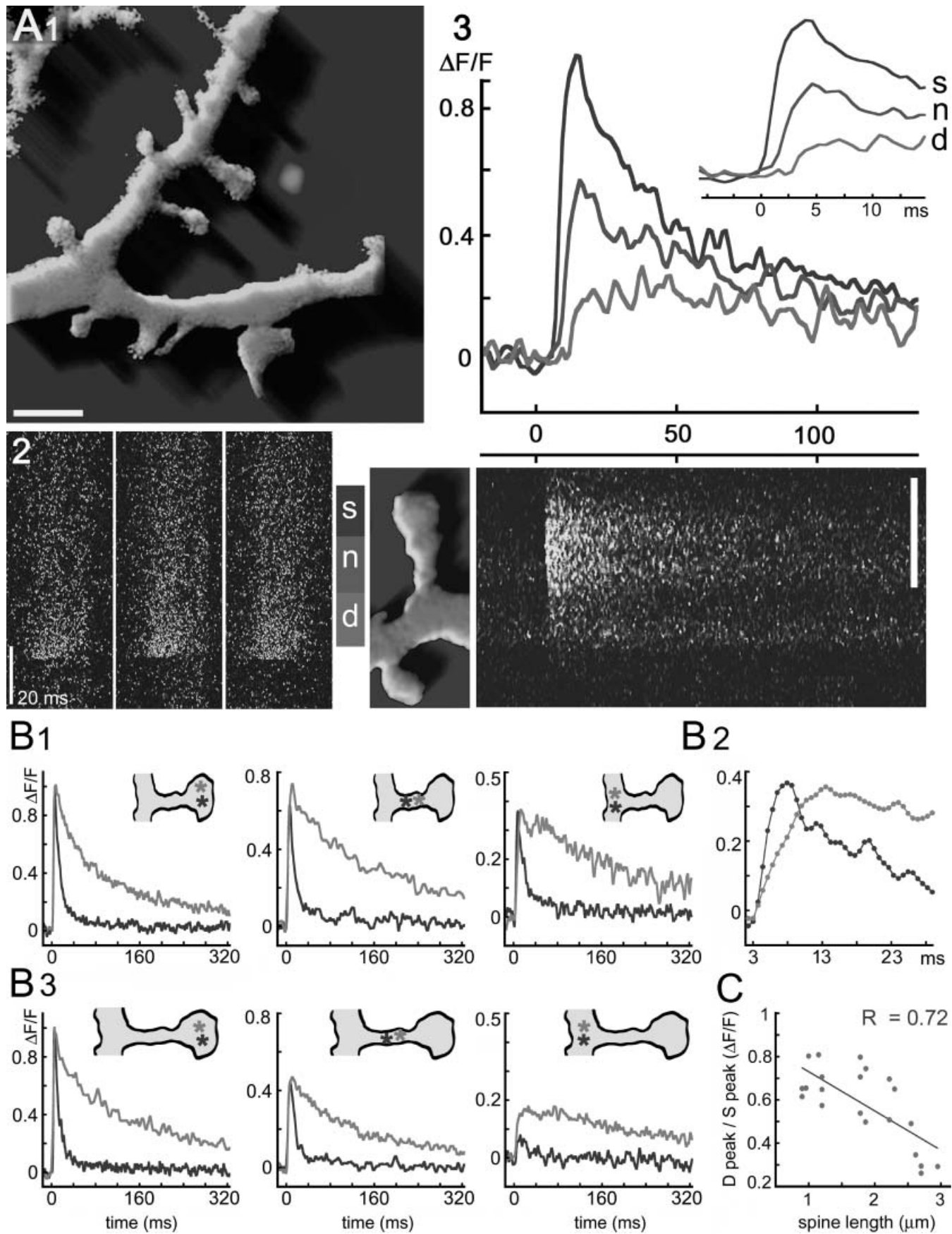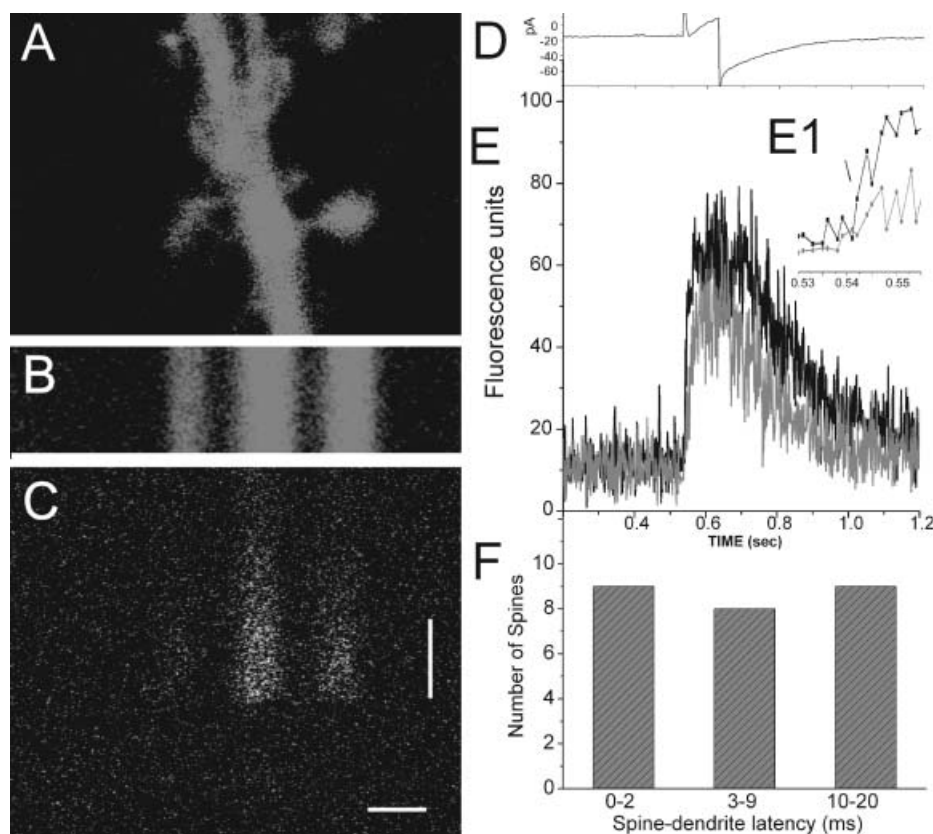
FIG. 6. Calcium transients produced by activation of calcium currents displayed a fast rise and slower removal kinetics. (A) Illustration of a dendritic segment with a large spine head, imaged with Alexa-Fluor 555. (B) An Alexa-Fluor 555 line scan through the spine head, on the right, a dendritic shaft, centre, and the thin spine, left. (C) Line scan of the Fluo-4 image, from bottom to top. Calcium current was evoked at 500 ms from the start of the line scan to produce a change in $[Ca^{2+}]_i$ in the parent dendrite, a smaller change in the right spine and a very small change in the left spine. (D) An illustration of the calcium current evoked in the soma for the same line scan shown in C. (E) The change in spine–dendrite $[Ca^{2+}]_i$ is presented as a function of time before and following the onset of calcium current. The two regions of interest comprise the calcium changes in the spine and parent dendrite. The recovery of $[Ca^{2+}]_i$ in the spine was fitted with a single exponential function with time constant of 177 ms. Insert (E1) is an expansion of the traces in E, to illustrate the fast rise time in the spine (light) and the parent dendrite (dark). A distinct delay in the spine response is indicated by an arrow. (F) The number of spines with short (0–2 ms), medium (3–9 ms) and long latency after the dendritic response. Only the first group can be considered independent of the dendritic response. Scale bars, 100 ms, 1 μm (A–C).

The rate of spine–dendrite coupling was correlated with changes in spine dimensions (Fig. 7F and G). Thus, 60% of the spines were completely isolated from the parent dendrite following their elongation by 0.3–0.5 μm (Fig. 7F). On average, elongation of spine necks produced a much larger effect on the spine–dendrite coupling than their shrinkage (Fig. 7G); shrinkage added at most 25% to the degree of coupling, but elongation reduced it by ∼ 85%.

Modelling and computation

To evaluate the ability of the dendritic spine to compartmentalize calcium and in particular to study the effect of the neck length, a one-dimensional model is presented in which we computed the ratio of

calcium ions pumped out in the neck spine to the ions reaching the dendrite. We showed that there exists a critical length, which separates dendritic spines into two classes. One class is the set of spines with long necks which can be considered to be isolated from their parent dendrites and the other class is the set of spines with short necks which can be considered part of the dendrite.

The model starts as follows: when calcium ions leave the spine head, their trajectories can be terminated in two ways; a free ion can reach the dendrite and be absorbed there or it can be extruded by a pump on its way out. To compute the ratio of the number of calcium ions leaving through the pumps to the number that reach the dendrite, we consider a model where the spine neck geometry is approximated by a one-dimensional interval $[0, L]$. The spine head is located at

FIG. 5. Uncaging of fluorescein produces fast onset, slow decaying increases in spine fluorescence. (A1) View of a 3-D reconstruction of a pDsRed-transfected neuron with dendrites and spines, and a dot (to the right of centre) to illustrate the size of the UV laser beam, similar to that shown in Fig. 1. (A2) Line scans of successive responses to flash photolysis of caged fluorescein, to show the consistency of the responses. (A3, bottom) Illustration of the spine–dendrite configuration, and the line scan running from left to right, of the response to flash photolysis in the spine head at time zero. (A3, top) Averaged changes in fluorescence within the different compartments, showing the distinct slow time course of reduction in fluorescence following the flash photolysis. Insert is a higher resolution image of the rise time in the different compartments. (B) Comparisons of fluorescence changes following uncaging of calcium (dark) and fluorescein (light), in the different compartments, in short (B1) and long (B3) spines. The decay time in all compartments is markedly prolonged for fluorescein compared to calcium in the short spines, although the rise time is slightly faster for the calcium response than the fluorescein one (B2). The difference between the responses to calcium and fluorescein is even more striking with the long spines (B3), where there is virtually no calcium response in the parent dendrite but a considerable response to fluorescein. (C) The dendritic response was linearly correlated with the spine neck length ($r = 0.72$, $P < 0.01$). Scale bar, 1 μm (A).
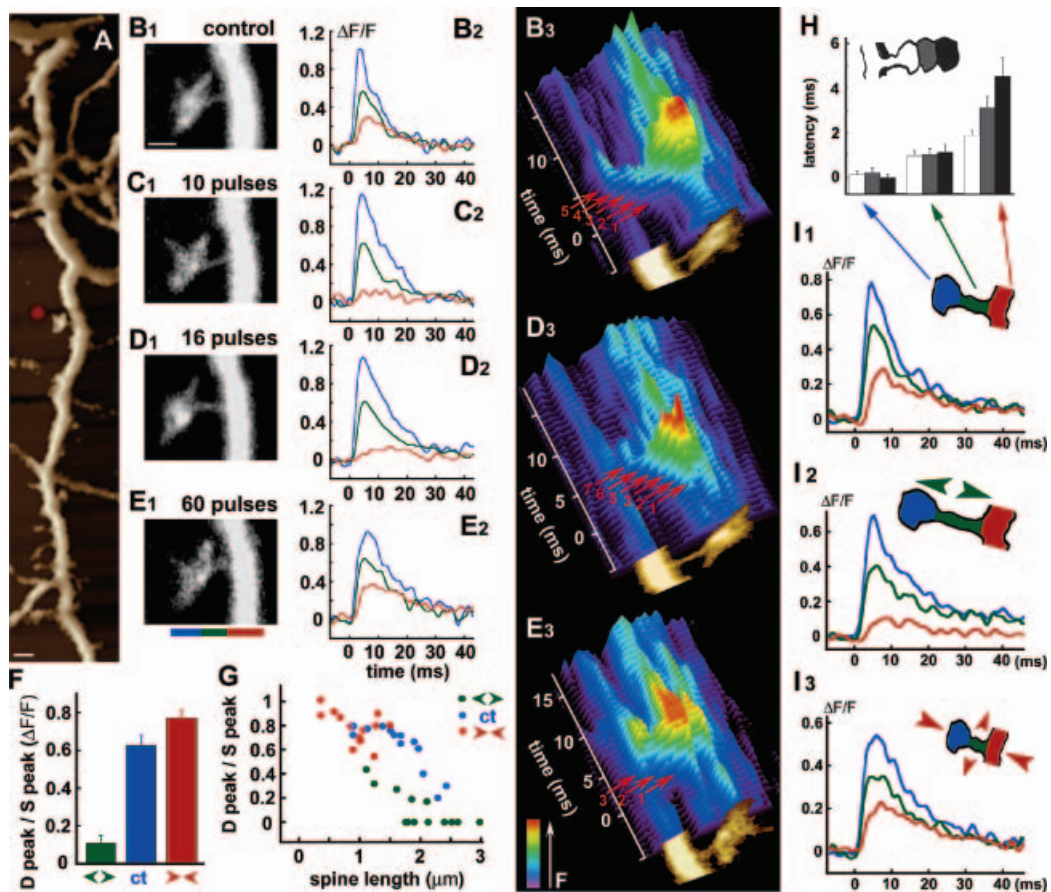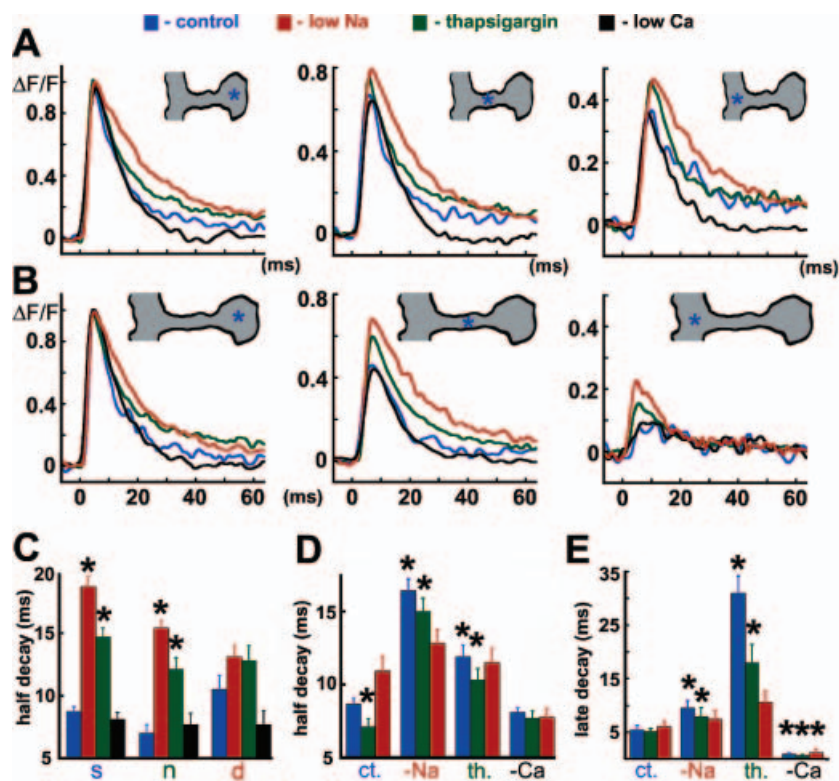
FIG. 7.

FIG. 8.

position $x = 0$ and the dendrite at position $x = L$. We assume for simplicity that the calcium pumps are uniformly distributed along the length of the spine neck. The calcium extrusion rate through the pumps is described by

$$J = -\frac{cX_m}{(c + K_{1/2})}, \tag{5}$$

where $K_{1/2}$ is the half-saturation constant of the pump and X_m is the maximum extrusion rate. We assume that $c \ll K_{1/2}$ so that the flux per pump becomes $J = -cX_m/K_{1/2}$. We note $\xi = X_m/K_{1/2}$ and if N_p denotes the total number of pumps then the calcium concentration c satisfies the reaction–diffusion equation

$$\frac{\partial c(x,t)}{\partial t} = D\frac{\partial^2 c(x,t)}{\partial x^2} - \xi N_p c(x,t) \quad \text{for } x \in [0, L], \tag{6}$$

with the initial condition $c(x, 0) = 0$, where the boundary conditions are:

$$\frac{\partial c(x,t)}{\partial n} = F(t) \quad \text{for } x = 0,$$

$$c(x,t) = 0 \quad \text{for } x = L.$$

The first boundary condition represents a flux $F(t)$ imposed at the location of the spine head and the second condition represents the absorption at the dendrite: when an ion reaches the dendrite, it cannot return to the spine neck.

The flux of the ions arriving at the dendrite is given by:

$$\Phi(t) = -D\frac{\partial c}{\partial x}\big|_{x=L} \tag{7}$$

whereas the total number of ions pumped out is given by:

$$P(t) = \int_0^L \xi N_p c(x,t) \mathrm{d}x. \tag{8}$$

Finally the ratio is given by:

$$R_L(t) = \frac{\Phi(t)}{P(t)} = -\frac{D\frac{\partial c}{\partial x}\big|_{x=L}}{\int_0^L \xi N_p c(x,t) \mathrm{d}x} \tag{9}$$

We evaluate $R(t)$, in the steady state regime, when $F(t) = C$ is a small constant. In this case equation 6 can be solved exactly and the solution is

$$p(x) = \frac{C}{2w\cosh(wL)}\left(\mathrm{e}^{w(x-L)} - \mathrm{e}^{-w(x-L)}\right) \tag{10}$$

where $w^2 = \chi/D$ and $\chi = \xi N_p$ and the constant ratio $r(L) = R_L(t)$ is given by

$$r(L) = \frac{1}{\cosh(wL) - 1}. \tag{11}$$

$r(L)$ depends on the length of the spine neck and the characteristic properties of the pumps. As L goes to zero $r(L)$ goes to infinity, that is, all ions arrive at the dendrite, asymptotically,

$$r(L) \sim_{L\to 0} \frac{C}{L^2}, \tag{12}$$

where the constant $C = 2/w^2$. On the other hand, for long spines, as L increases, asymptotically,

$$r(L) \sim_{L\to\infty} 2\mathrm{e}^{-wL}. \tag{13}$$

The two different asymptotic behaviours prove that the length of a spine neck is a critical parameter; we prove below that spine length should be considered a low pass filter that stops conducting calcium ions after a critical length. Indeed, when L exceeds such lengths, almost all calcium ions are extruded through the neck pumps.

The characteristic length L_c can be defined as the inflection point of the curve $L \to R_L$, where the graph is the closest to the origin. The characteristic length L_c is defined at the only solution of the variational problem

FIG. 7. Spine–dendrite coupling is continuously modified. (A) A dendritic segment with one spine that was extensively studied, near the red dot. (B) Control condition, where a transient response in the spine head is followed by a medium calcium transient in the parent dendrite. In B3, numbered arrows indicate scanned lines where threshold responses are seen. (B1) Image, (B2) analysed line scans, (B3) fast 3-D rendering image of the spine–dendrite to show the leak of calcium from the spine to the dendrite on a line-by-line sequence. (C–E) The same spine, after (C) 10 flashes, (D) 16 flashes and (E) 60 flashes. Note that the spine shrank and that the parent dendrite then responded to the calcium surge produced in the spine head (E3). (F and G) Changes in individual spine length are associated with a change in coupling index [dendritic peak ($\Delta F/F$)/spine peak ($\Delta F/F$)]. Blue, red and green circles represent control, shrunken and elongated spines, respectively, for the same group of 13 spines. Note that only those spines are represented for which both shrinkage and elongation have been found (outward-pointing arrow heads, elongation; inward-pointing, shrinkage). (H) The spine compartments had different latencies depending on spine neck length, with the longest latency being in the parent dendrite of the longest spines (green). (I) Grouped data of spines in control conditions ($n = 25$, I1), top, elongated ($n = 16$, I2) and shrunk spines ($n = 19$, I3), illustrating the change in response of the parent dendrites (red curves) to the change in length of the spines.

FIG. 8. The dynamics of calcium transients depends on influx into stores and removal through a Na–Ca exchanger. (A and B) Averages of calcium transients in (left) spine heads, (middle) neck and (right) dendrite, in control (blue) and in the three treatment groups: low Na (red, $n = 15$ and 16 for (A) short and (B) long spines, respectively), thapsigargin (green, $n = 16$ and 18) and low $[Ca^{2+}]_o$ (black, $n = 6$ and 5). The decay kinetics in the spines were markedly slowed by both thapsigargin and low $[Na]_o$ but were sped up by low $[Ca^{2+}]_o$. The effects of the treatments are more pronounced on the decay kinetics, as well as on the size of the responses, in the necks and parent dendrites of long spines. (C) A quantitative analysis of the half-decay times in the three compartments: s, spine; n, neck; and d, dendrite, showing a significant (*$P < 0.01$) increase in decay time primarily in the spine head of the low Na- and thapsigargin-treated cultures. (D) Same data as in C, grouped by the treatment, illustrating for each treatment the decay in the spine head (blue), spine neck (green) and dendrite (red); th, thapsigargin. (E) Analysis of the late decay of the responses shows marked deviations from control: in the presence of thapsigargin (th) the decay was significantly prolonged, whereas low $[Ca^{2+}]_o$ caused a marked speeding up of the recovery. The vertical scale is the time for recovery, with zero time at 30 ms after the onset of the calcium response. Same colour code as in D.

$$L_c = \underset{L>0}{Arg\ \min}\{L^2 + r^2(L)\} \qquad (14)$$

and if we denote $x = wL$ the minimal value for x is given by

$$x = \frac{\sinh(x)}{(\cosh(x) - 1)^3} \qquad (15)$$

and the nonzero solution is

$$wL = x = 1.3751. \qquad (16)$$

From equation 16 the critical length above which the spine stops conducting calcium ions to the dendrite can be computed, given the pump density, and

$$L_c = \frac{1.3751\sqrt{D}}{\sqrt{\xi N_p}}. \qquad (17)$$

For $X_m = -15\ \mu\text{M/s}$, $K = 0.9\ \mu\text{M}$ and $D = 400\ \mu\text{m}^2/\text{s}$ then $\xi = 16.66$ and a cutoff length at $L = 1.5\ \mu\text{m}$ determines that $N_p = 20$. For $L > L_c$ the spine is isolated and for $L < L_c$ the spine is coupled to the dendrite.

Note that the extrusion flux time scale was reported to be $1600/\text{s}$ (in Sabatini *et al.*, 2002), from which we conclude that the number of pumps that produce a ratio of $\xi = 16.66$ should be ~ 100. Compared to N_p, this proves that a spine becomes isolated when $1/4$ of the pumps are located on the spine neck.

Calcium removal

The marked difference in decay time constants between calcium and fluorescein indicates that active processes contribute to the fast removal of excess calcium. This could take place either by uptake of calcium into stores or by extrusion out to the extracellular space. We examined the two possibilities by studying the kinetics of calcium decay in cultures treated with thapsigargin, which blocks entry of calcium into the stores, and by removal of sodium from the recording medium, which interferes with the Na–Ca exchanger, a major calcium extrusion mechanism. We also studied the effects of removal of calcium from the recording medium, which causes a gradual depletion of the stores.

While the peak amplitudes of the calcium transients were about the same in all treatments and controls, both thapsigargin and low $[\text{Na}]_o$ medium caused a significant slowing of the decay of the calcium transient at the spine head (Fig. 8A and B). The effects of the treatments were especially pronounced in the long spines: the half-time of decay for the thapsigargin-treated group was 11.5 ± 1.1 ms ($n = 18$; $P < 0.03$ compared to controls which were 8.75 ± 0.35 ms; see above), and was 18.3 ± 1.3 ($n = 16$, $P < 0.01$) for the low $[\text{Na}]_o$. The effects of these treatments on the short spines were smaller than on the long ones (Fig. 8A and B). Interestingly, removal of $[\text{Ca}^{2+}]_o$ sped up only slightly the decay time of the elevated $[\text{Ca}^{2+}]_i$. These effects were pronounced at the spine head compartment. The similar $[\text{Ca}^{2+}]_i$ decay kinetics in the absence of $[\text{Ca}^{2+}]_o$ indicates that the initial rate of entry into the stores in the spine head is not governed by existing calcium in these stores. However, the later phase of the recovery from the calcium load was significantly accelerated by the absence of extracellular calcium (Fig. 8E).

A reduction in efficacy of calcium removal mechanisms caused the enhancement of responses of the parent dendrite to a rise in $[\text{Ca}^{2+}]_i$, especially in long spines (Fig. 8B), where a reduction in $[\text{Na}]_o$ or the presence of thapsigargin enhanced significantly (*t*-test, $P < 0.01$) the responses in the parent dendrite compared to control, indicating that, in the absence of removal mechanisms, calcium tended to diffuse further into the dendrite (Fig. 8B, right). The effect of low Na was particularly pronounced in the spine necks; in control conditions the decay at the spine necks was faster than that of the spine heads, especially in spines with large heads (Fig. 8E). Thapsigargin and especially low $[\text{Na}]_o$ increased neck responses, indicating that a Na–Ca exchanger is more involved in faster Ca decay in spine necks. The effect of blocking the Na–Ca exchanger could be seen at the very early stages of calcium removal (Fig. 8C and D): the half-decay of calcium in spine head and neck was more than twice as slow as in control. The later stages of decay were less affected by removal of Na (Fig. 8E). On the other hand, thapsigargin affected significantly the slower component of $[\text{Ca}^{2+}]_i$ decay, making the rate of late decay more than five times slower in the spine head and three times slower in the neck (Fig. 8E).

Discussion

The present results indicate that spine neck length controls the magnitude of spine–dendrite communication, not so much by virtue of the size of the intracellular space in the spine neck, as there is little difference between short and long spines with respect to diffusion of uncaged fluorescein, but by the presence of active calcium removal mechanisms in this compartment. Previous studies, which used fluorescent molecules to estimate the free diffusion between the spine head and the parent dendrite, concluded that this axis is of low resistance, because the equilibration of diffusive particles between spine and dendrite is rather fast (Svoboda *et al.*, 1996). We confirm these results with respect to fluorescein, to show that there are no apparent barriers to the arrival of elevated fluorescence evoked in the spine head to the parent dendrite and the longer spines are merely slower in arrival of fluorescein to the parent dendrite. On the other hand, the impact of the elevated calcium is highly dependent on spine length, probably due to the fast calcium removal mechanisms which may reduce drastically the concentration of free calcium available for diffusion from the longer spine heads into the parent dendrite. In this respect, the spine neck can be considered an active filter for the passage of calcium ions from the spine head to the parent dendrite compartment.

In the one-dimensional model of the spine neck presented here we demonstrate that, for a given concentration of pumps, there exists a critical length above which the spine loses its ability to conduct calcium ions and can therefore be considered to be isolated from the parent dendrite. The transition from a conducting to an isolated spine can be achieved by increasing the number of pumps in the spine neck. We predict that adding one or two pumps may be sufficient which suggests that, for a given pump concentration, changing the spine neck causes a sharp transition from isolated to conducting spines.

From equations 16 and 17 we conclude that a dendritic spine can become isolated in two different ways: one is to increase the spine neck length and the other is to increase the number of pumps. However, these two procedures are not equivalent because the number of pumps has to increase quadratically in order to produce a similar effect to a linear change in spine length.

Because a dendrite is a stable structure whereas a dendritic spine is flexible, having the ability to change its length, only dendritic spines can be coupled and/or uncoupled dynamically by changing both the neck length and the number of pumps. Comparing the time needed for a pump to be functionally active after being synthesized with the time to change the spine geometry, our computation suggests that it is more

efficient and faster for the spine head to be compartmentalized by increasing the length rather than adding pumps.

Finally, it is possible to estimate the effect of changing the spine neck length from equation 11. Indeed for $L = 1.5$ μm and $N_p = 20$, the ratio of pumped ions to ions arriving in the dendrite), $r(1.5) = 0.95$, that is, for 10 ions pumped out, 9 arrive in the dendrite whereas for $L = 1$ μm, $r(1) = 2.33$, that is, for 10 ions pumped out, 23 arrive in the dendrite.

The calcium removal mechanisms available at the spine head are apparently very important for increases in $[Ca^{2+}]_i$ as well as the removal of excess $[Ca^{2+}]_i$. Calcium can be released from stores, has been shown to be available in spine heads (Korkotian & Segal, 1998 Volfovsky et al., 1999), and may even contribute to a synaptically induced rise in free $[Ca^{2+}]_i$ (Emptage et al., 1999). The removal mechanisms include calcium binding proteins, calcium stores, pumps and exchangers. Interestingly, the spines do not contain mitochondria, the largest calcium stores in the cell. We have found that both stores and a Na–Ca exchanger may contribute to the removal mechanisms of elevated $[Ca^{2+}]_i$ but that they do not contribute to the initial rise in $[Ca^{2+}]_i$. We did not try to block all removal mechanisms together as this procedure was found to be very stressful for the cell and is also associated with morphological changes of the spines, which will complicate the interpretation of these results.

Calcium can diffuse from the spine head to the parent dendrite but it can also diffuse from the parent dendrite to the spine head. In an earlier study, spines were found to be resistant to influx of calcium from the parent dendrite but no distinction was made between short and long ones (Guthrie et al., 1991). It is likely that, with rather poor resolution, spines could be unequivocally identified as such primarily if they were long ones. Such might also be the case with current estimates of spine independence, where short spines cannot be clearly resolved. In any case, we tested the diffusion of photolysed calcium from the parent dendrite into the spine head and found that it has about the same kinetics as that of calcium diffusion from the spine head into the parent dendrite (our unpublished observations). Taken together with our observations on the transient calcium changes that accompany soma-evoked calcium current, and considering the speed of calcium diffusion between the two compartments, a cautious interpretation of the assertion that spines possess voltage-gated calcium channels is in order: when a delay of 2–3 ms is found between the transient in the parent dendrite and the spine head, it is not certain that the spine head possess voltage-gated calcium channels, as it is likely that the transient seen in the spine head originates in the parent dendrite. In fact, in our conditions it appears that only a third of the spines could evoke a response that was < 3 ms in latency after the the dendritic response.

The decay of the elevated $[Ca^{2+}]_i$ in the present study, < 9 ms, is the fastest among similar values computed elsewhere and closest to the extrapolated value calculated by Sabatini et al. (2002). This value is far shorter than what we (Fig. 8) and others (e.g. Majewska et al., 2000a) have seen for back-propagating action potentials or calcium currents. The reasons for this difference may reflect the low concentration of the buffer used in the present study, 2–3 μM, making it virtually transparent to the rest of the buffering capacity of the cell. Also, it may reflect the fact that the uncaging of calcium is a discrete and true point source, unlike the case of a synaptic event where the calcium response may also reflect the binding kinetics of the transmitter and the ion channel opened by the depolarization. This may simplify the estimation of diffusion and removal mechanisms.

The possibility that the changes in fluorescence that we observe in the parent dendrite are a function of diffusion of the bound calcium or dye was examined in the current study, using several complementary methods. We confirmed previous observations by Majewska et al.

(2000b), using recovery from bleaching, to show that the dye actually diffuses more slowly than $[Ca^{2+}]_i$ between the parent dendrite and the spine head. Also, the use of a membrane-bound calcium-fluorescent dye clearly indicates that it is $[Ca^{2+}]_i$ that travels between the spine head and the parent dendrite. One other possibility which we did not examine is that calcium is bound to an innate carrier which helps the ion traverse the spine neck.

Spine length is in a dynamic state and can be modified by recent transient elevations of $[Ca^{2+}]_i$ in the spine head. Previous studies have demonstrated that the spine head is motile, morphing continuously in the absence of intense afferent activity, whereas glutamate activation of the spine head causes its arrest and eventual shrinkage (Fischer et al., 1998; Korkotian & Segal, 2001). It was proposed that the variations in spine form underlie spine calcium dynamics, but this was demonstrated only in a subset of shrinking spines (Majewska et al., 2000b). More recent studies assume that spines with larger heads have a higher concentration of glutamate receptors and thus are likely to produce larger responses than those with a smaller head (Matsuzaki et al., 2001). We could not establish a correlation between the size of the spine head and the magnitude or time course of responses to uncaging of calcium, indicating that, while the number of membrane receptors may depend on the size of the spine head, intrinsic mechanisms related to calcium stores and removal of free calcium are probably not dependent on spine size. On the other hand, spine length, which varies considerably depending on the recent history of the spine, can affect the spine communication with the parent dendrite in a bidirectional manner. Because many synaptic processes are affected by calcium-dependent phosphorylation and dephosphorylation of synaptic proteins, this variable link between spines and dendrites should have a major impact on synaptic plasticity.
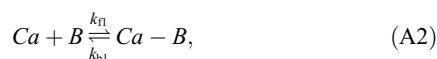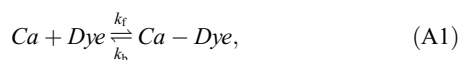
Acknowledgements

References

Brown, E.B., Shear, J.B., Adams, S.R., Tsien, R.Y. & Webb, W.W. (1999) Photolysis of caged calcium in femtoliter Volumes using two photon excitation. *Biophys. J.*, **76**, 489–499.

Delaney, K.R. & Zucker, R.S. (1990) Calcium released by photolysis of DM-nitrophen stimulates transmitter release at squid giant synapse. *J. Physiol. (Lond.)*, **426**, 473–498.

Emptage, N., Bliss, T.V. & Fine, A. (1999) Single synaptic events evoke NMDA receptor-mediated release of calcium from internal stores in hippocampal dendritic spines. *Neuron*, **22**, 115–124.

Felmy, F., Neher, E. & Schneggenburger, R. (2003) The timing of phasic transmitter release is Ca^{2+} dependent and lacks a direct influence of presynaptic membrane potential. *Proc. Natl Acad. Sci. USA*, **100**, 15200–15205.

Fischer, M., Kaech, S., Knutti, D. & Matus, A. (1998) Rapid actin based plasticity in dendritic spines. *Neuron*, **20**, 847–854.

Goldin, M., Segal, M. & Avignone, E. (2001) Functional plasticity triggers formation and pruning of dendritic spines in cultured hippocampal networks. *J. Neurosci.*, **21**, 186–193.

Grigoriev, I., Makhnovskii, A., Berezhkovskii, A. & Zitserman, V. (2002) Kinetics of escape through a small hole. *J. Chem. Physics*, **116**, 9574–9577.

Guthrie, P.B., Segal, M. & Kater, S.B. (1991) Independent regulation of calcium revealed by imaging dendritic spines. *Nature*, **354**, 76–80.

Harris, K.M. & Kater, S.B. (1994) Dendritic spines: cellular specializations imparting both stability and flexibility to synaptic function. *Annu. Rev. Neurosci.*, **17**, 341–371.

Holcman, D., Schuss, Z. & Korkotian, E. (2004) Calcium dynamics in dendritic spines. *Biophys. J.*, **87**, 81–91.

Korkotian, E., Oron, D., Silberberg, Y. & Segal, M. (2004) Confocal microscopic imaging of fast uv-laser photolysis of caged compounds. *J. Neurosci. Meth.*, **133**, 153–159.

Korkotian, E. & Segal, M. (1998) Fast confocal imaging of calcium released from stores in dendritic spines. *Eur. J. Neurosci.*, **10**, 2076–2084.

Korkotian, E. & Segal, M. (1999) Bidirectional regulation of dendritic spine dimensions by glutamate receptors. *Neuroreport*, **10**, 2875–2877.

Korkotian, E. & Segal, M. (2001) Spike-associated fast twitches of dendritic spines in cultured hippocampal neurons. *Neuron*, **30**, 751–758.

Majewska, A., Brown, E., Ross, J. & Yuste, R. (2000a) Mechanisms of calcium decay kinetics in hippocampal spines: Role of spine calcium pumps and calcium diffusion through the spine neck in biochemical compartmentalization. *J. Neurosci.*, **20**, 1722–1734.

Majewska, A., Tashiro, A. & Yuste, R. (2000b) Regulation of spine calcium dynamics by rapid spine motility. *J. Neurosci.*, **20**, 8262–8268.

Matsuzaki, M., Ellis-Davies, G.C.R., Nemoto, T., Miyashita, Y., Iino, M. & Kasai, H. (2001) Dendritic spine geometry is critical for AMPA receptor expression in hippocampal CA1 pyramidal neurons. *Nature Neurosci.*, **4**, 1086–1092.

Nimchinsky, E.A., Sabatini, B.L. & Svoboda, K. (2002) Structure and function of dendritic spines. *Annu. Rev. Physiol.*, **64**, 313–353.

Pilpel, Y. & Segal, M. (2004) Activation of PKC induces rapid morphological plasticity in dendrites of hippocampal neurons via rac- and rho-dependent mechanisms. *Eur. J. Neurosci.*, **19**, 3151–3164.

Sabatini, B.L., Oertner, T.G. & Svoboda, K. (2002) The life cycle of Ca²⁺ ions indendritic spines. *Neuron*, **33**, 439–452.

Segal, M. (1995) Fast imaging of [Ca]i reveals presence of voltage gated calcium channels in dendritic spines of cultured hippocampal neurons. *J. Neurophysiol.*, **74**, 484–488.

Segal, M., Korkotian, E. & Murphy, D.D. (2000) Dendritic spine induction and pruning - common cellular mechanisms? *Trends Neurosci.*, **23**, 53–57.

Shepherd, G.M., (1996) The dendritic spine. A multifunctional integrative unit. *J. Neurophysiol.*, **75**, 2197–2210.

Smith, G., Dai, L., Miura, R. & Sherman, A. (2001) Asymptotic analysis of buffered calcium diffusion near a point source. *SIAM J. Appl. Math.*, **61**, 1816–1838.

Svoboda, K., Tank, D.W. & Denk, W. (1996) Direct measurement of coupling between dendritic spines and shafts. *Science*, **272**, 716–719.

Volfovsky, N., Parnas, H., Segal, M. & Korkotian, E. (1999) Geometry of dendritic spines affects calcium dynamics in hippocampal neurons: theory and experiments. *J. Neurophysiol.*, **82**, 450–462.

Yuste, R. & Denk, W. (1995) Dendritic spines as basic functional units of neuronal integration. *Nature*, **375**, 682–684.

Appendix

Model

We present here a crude model to evaluate the time course and bound : free proportion for calcium ions to equilibrate with endogenous buffer (calmodulin) and exogenous dye molecules (Fluo-4) distributed uniformly. The chemical kinetic equations describing the binding of calcium ions to the dye molecules and buffers are

$$Ca + Dye \underset{k_b}{\overset{k_f}{\rightleftharpoons}} Ca - Dye, \tag{A1}$$

$$Ca + B \underset{k_{b1}}{\overset{k_{f1}}{\rightleftharpoons}} Ca - B, \tag{A2}$$

where k_f, k_{f1} and k_b, k_{b1} are, respectively, the forward and backward binding rate constants for the dye and buffer molecules. We ignored here calcium pumps and exchangers because they will simply reduce the amount of free calcium in the computation of the equilibration time scale.

The chemical kinetic equations are

$$\frac{d[Ca - Dye]}{dt} = k_f[Ca][Dye] - k_b[Ca - Dye], \tag{A3}$$

$$\frac{d[Ca - B]}{dt} = k_f[Ca][B] - k_b[Ca - B]. \tag{A4}$$

and the characteristic time becomes

$$T_a = \frac{1}{k_f[Dye] + k_{f1}[B] + k_b + k_{b1}}. \tag{A5}$$

For $[Dye] = 2$ μM, $k_b = 170/s$, $k_f = 60$ μM⁻¹s⁻¹, $[B] = 1$ μM, $k_{b1} = 250/s$, $k_{f1} = 250$ μM⁻¹s⁻¹ (see Smith *et al.*, 2001). The association time is

$$T_a = 0.5 \, \text{ms}. \tag{A6}$$

This time constant T_a has to be compared with the mean time constant, $\tau_1 = 6.5$ ms, taken for the calcium ions to find the entrance to the neck.

When the equilibrium state is achieved between Fluo-4, endogenous buffers and the free calcium ions, the ratio of free calcium : bound calcium is given by

$$\frac{[Ca]}{[Ca - Dye] + [Ca - B]} = \frac{1}{K_D[D] + K_B[B]}, \tag{A7}$$

where the dye dissociation constant $K_D = k_f/k_b$ and the buffer dissociation constant $K_B = k_{f1}/k_{b1}$. The ratio of calcium bound to Fluo-4 molecules : calcium bound to calmodulin is given by

$$\frac{[Dye - Ca]}{[B - Ca]} = \frac{K_D[B]}{K_B[Dye]}. \tag{A8}$$

A numerical computation of this ratio gives a value of 0.015. Although there is a large variability of the forward and backward binding rates in the literature for calmodulin, the mean of the equilibrium constant K_B is 1 μM. Using the above numerical values, the ratio of the free calcium : bound calcium is $[Ca]/\{[Ca - Dye] + [Ca - B]\}$, equal to 0.58. Thus, for 100 calcium ions, 37 are free. If the concentration of calmodulin is neglected, the binding ratio $[Ca]/[Ca - Dye]$ equals 1.43, so that 70 of 100 calcium ions are free.

The computation given above lets us estimate approximately the calcium fraction which stays free in the presence of 2 μM Fluo-4. We assume that not less than 40% of calcium ions diffuse alone.

As in our computations above we used a concentration of Fluo-4 similar to that used under experimental conditions (Figs 1 and 2 and Table 1), we conclude that the amount of free calcium consists of a significant part of its total amount.

TABLE A1. Parameter values

Parameter	Description	Value
D_{Ca2+}	Diffusion constant of calcium ions	400 μm²/s[‡]
k_f	Forward binding rate for Fluo-4	60 μM⁻¹s⁻¹[†]
k_b	Backward binding rate for Fluo-4	170 s⁻¹[†]
k_{f1}	Forward binding rate for calmodulin	250 μM⁻¹s⁻¹[‡]
k_{b1}	Backward binding rate for calmodulin	250 s⁻¹[‡]
$[B]$	Calmodulin concentration	1 μM
$[Dye]$	Dye molecule concentration	2 μM
ξ	Time constant of pumps	16.66 s⁻¹[‡]
X_m	Maximum extrusion rate	15 μM⁻¹s⁻¹[‡]
$K_{1/2}$	Half-saturation constant	0.9 μM[‡]
k_b	Backward binding rate for Fluo-4	170 μM⁻¹s⁻¹[†]

[†]Holcman *et al.* (2004); [‡]Smith *et al.* (2001).

Time scales and effect of buffers

The free diffusion time scale is given by $\tau = \tau_1 + \tau_2 = V/4D\varepsilon + L^2/2D$ while, in the presence of N_{binding} buffer molecules, the arrival time delay is given by $\tau = 7.75 + N_{\text{binding}} \cdot k_{\text{b1}}$. From this formula, the number of bound calcium ions can be computed, once the delay is measured.

In any case, the presence of buffer molecules in the spine head influence the dynamic of calcium inside the spine neck. The impact of endogenous buffers on calcium dynamics has been studied by Holcman *et al.* (2004) when calcium ions were entering through some channels located at the top of the spine head, but the present situation is different because the calcium ions freed by the uncaging process are spread throughout the spine head.